Far-field measurement of ultra-small plasmonic mode volume

Shuang Zhang,[1] Yong-Shik Park,[1] Yongmin Liu,[1] Thomas Zentgraf[1] and Xiang Zhang[1,2*]

[1] Nanoscale Science and Engineering Center, 3112 Etcheverry Hall, University of California, Berkeley, California 94720, USA
[2] Materials Sciences Division, Lawrence Berkeley National Laboratory, 1 Cyclotron Road, Berkeley, California 94720, USA
*xiang@berekeley.edu

Abstract: Light-matter interaction can be greatly enhanced in nano-scale plasmonic cavities with tightly confined optical mode, where the mode volume determines the interaction strength. The experimental determination of the mode volume of plasmonic elements is therefore of fundamental importance. Mapping the electric field distribution using near-field scanning optical microscopy (NSOM) may disturb the field distribution hence prevent a reliable measurement of the mode volume. Here, we develop a non-pertubative technique to experimentally determine the mode volume of plasmonic resonators in the far field through a unique optical force method.

©2010 Optical Society of America

OCIS codes: (250.5403) Plasmonics; (310.6628) Subwavelength structures, nanostructures.

References and links

1. E. Prodan, C. Radloff, N. J. Halas, and P. Nordlander, "A hybridization model for the plasmon response of complex nanostructures," Science **302**(5644), 419–422 (2003).
2. K. R. Li, M. I. Stockman, and D. J. Bergman, "Self-similar chain of metal nanospheres as an efficient nanolens," Phys. Rev. Lett. **91**(22), 227402 (2003).
3. K. B. Crozier, A. Sundaramurthy, G. S. Kino, and C. F. Quate, "Optical antennas: Resonators for local field enhancement," J. Appl. Phys. **94**(7), 4632 (2003).
4. P. J. Schuck, D. P. Fromm, A. Sundaramurthy, G. S. Kino, and W. E. Moerner, "Improving the mismatch between light and nanoscale objects with gold bowtie nanoantennas," Phys. Rev. Lett. **94**(1), 017402 (2005).
5. P. Mühlschlegel, H. J. Eisler, O. J. F. Martin, B. Hecht, and D. W. Pohl, "Resonant optical antennas," Science **308**(5728), 1607–1609 (2005).
6. A. Alú, and N. Engheta, "Tuning the scattering response of optical nanoantennas with nanocircuit loads," Nat. Photonics **2**(5), 307 (2008).
7. A. Alù, and N. Engheta, "Input impedance, nanocircuit loading, and radiation tuning of optical nanoantennas," Phys. Rev. Lett. **101**(4), 043901 (2008).
8. J. N. Farahani, D. W. Pohl, H. J. Eisler, and B. Hecht, "Single quantum dot coupled to a scanning optical antenna: a tunable superemitter," Phys. Rev. Lett. **95**(1), 017402 (2005).
9. R. M. Bakker, V. P. Drachev, Z. T. Liu, H. K. Yuan, R. H. Pedersen, A. Boltasseva, J. J. Chen, J. Irudayaraj, A. V. Kildishev, and V. M. Shalaev, J. Irudayaraj A. V. Kildishev, V. Alexander, and V. M. Shalaev, "Nanoantenna array-induced fluorescence enhancement and reduced lifetimes," N. J. Phys. **10**(12), 125022 (2008).
10. D. J. Bergman, and M. I. Stockman, "Surface plasmon amplification by stimulated emission of radiation: quantum generation of coherent surface plasmons in nanosystems," Phys. Rev. Lett. **90**(2), 027402 (2003).
11. N. I. Zheludev, S. L. Prosvirnin, N. Papasimakis, and V. A. Fedotov, "Lasing spaser," Nat. Photonics **2**(6), 351–354 (2008).
12. E. M. Purcell, "Spontaneous emission probabilities at radio frequencies," Phys. Rev. **69**, 681 (1946).
13. O. Painter, R. K. Lee, A. Scherer, A. Yariv, J. D. O'Brien, P. D. Dapkus, and I. Kim I, "Two-dimensional photonic band-Gap defect mode laser," Science **284**(5421), 1819–1821 (1999).
14. K. J. Vahala, "Optical microcavities," Nature **424**(6950), 839–846 (2003).
15. S. Maier, "Effective mode volume of nanoscale plasmon cavities," Opt. Quantum Electron. **38**(1-3), 257–267 (2006).
16. T. Klar, M. Perner, S. Grosse, G. von Plessen, W. Spirkl, and J. Feldmann, "Surface-plasmon resonances in single metallic nanoparticles," Phys. Rev. Lett. **80**(19), 4249–4252 (1998).
17. T. Zentgraf, J. Dorfmüller, C. Rockstuhl, C. Etrich, R. Vogelgesang, K. Kern, T. Pertsch, F. Lederer, and H. Giessen, "Amplitude- and phase-resolved optical near fields of split-ring-resonator-based metamaterials," Opt. Lett. **33**(8), 848–850 (2008).

18. M. L. Povinelli, S. G. Johnson, M. Lonèar, M. Ibanescu, E. J. Smythe, F. Capasso, and J. D. Joannopoulos, "High-Q enhancement of attractive and repulsive optical forces between coupled whispering-gallery- mode resonators," Opt. Express **13**(20), 8286–8295 (2005).
19. M. L. Povinelli, M. Loncar, M. Ibanescu, E. J. Smythe, S. G. Johnson, F. Capasso, and J. D. Joannopoulos, "Evanescent-wave bonding between optical waveguides," Opt. Lett. **30**(22), 3042–3044 (2005).
20. S. W. Chang, C. Y. A. Ni, and S. L. Chuang, "Theory for bowtie plasmonic nanolasers," Opt. Express **16**(14), 10580–10595 (2008).
21. S. Linden, C. Enkrich, M. Wegener, J. F. Zhou, T. Koschny, and C. M. Soukoulis, "Magnetic response of metamaterials at 100 terahertz," Science **306**(5700), 1351–1353 (2004).
22. H. E. Kamchouchi, and A. A. Zaky, "A direct method for calculation of the edge capacitance of thick electrodes," J. Phys. D Appl. Phys. **8**(12), 1365–1371 (1975).
23. E. W. Greeneich, "An analytical model for the gate capacitance of small-geometry MOS structures," IEEE Trans. Electron. Dev. **30**(12), 1838–1839 (1983).

Plasmonics offer the optical interfacing between free space radiation and the nano world [1,2]. Among various plasmonic designs, optical nano-antennas are of special interest since they are capable of focusing light into a small gap region with nanometer scales in all three dimensions, and can be tailored to operate at various frequency bands [3–7]. Besides their usual antenna functionalities such as transmitting and receiving signals, optical antennas also behave as ultra-small plasmonic resonators which can be used to strongly increase light-matter interaction. In particular, incorporating gain medium to the tightly confined mode ('hot-spot') facilitates applications such as efficient light emitting devices, enhanced spontaneous emission and nano-lasers [8–11], thanks to the Purcell effect [12] which is proportional to the ratio between the quality factor Q and the mode volume V. This is to say, the ultra-small mode volume can compensate for a relatively low quality factor in an optical antenna, resulting in a Purcell factor that may exceed other optical systems such as photonic defect modes [13] and high Q cavity ring resonators [14].

Determination of the mode volume is therefore of great importance for optimal design of active plasmonic devices and prediction of performance of nano-emitters positioned at a cavity's 'hot-spot' [15]. However, it cannot be simply deduced from its geometry and normally requires 3D near-field measurement of the electric field distribution. While recent progress in the technology of NSOM has allowed the probing of near field pattern in the nanometer scale [16,17], the perturbation of the NSOM tip to the intrinsic field distribution makes the measurement of the original mode volume very difficult, not to mention the technical challenges associated with mapping the magnitude of the field in all three dimensions.

In this work, we develop a method for measuring deep sub-wavelength mode volume of plasmonic antennas by simply detecting the far-field signal without introducing any mode perturbation. This is accomplished by an optical force analysis that converts the far-field attainable spectral information to the near-field electric field information through a differentiation method. More specifically, the sensitivity of the resonance to a small change of resonator geometry is directly related to the magnitude of the optical force exerted locally at the displaced part, which, in an electrostatic picture, can be considered as a Coulomb force due to the charge accumulation at this particular region. Furthermore, the Coulomb force can be related to the local electric field amplitude and hence the mode volume of the resonator. This method complies with a basic physical principle, stressing that the stronger an optical mode is confined within a cavity, the more sensitive the resonance of the system is to the changes of the material or structural parameters at the "hot spot".

We start by formulating the relations between the resonator mode volume and the sensitivity of the resonance frequency to a geometrical change at the 'hot spot'. We consider an optical antenna with a feeding gap size g (see Fig. 1). The resonance frequency difference $\Delta\omega$ resulting from a small change in the gap sizes Δg is directly related to the optical force *per photon* between the two metal facets across the feeding gap [18,19] [Fig. 1(a)],

$$F = -\frac{\Delta U}{\Delta g} = -\hbar \frac{\Delta\omega}{\Delta g} \tag{1}$$

where U is the photon energy in the antenna and $\hbar$ is the reduced Planck constant. Here, the force is defined to be positive if it is along the direction of increasing gap size.

For gap sizes in the deep sub-wavelength scale, the quasi-static picture can be applied for the gap region [Fig. 1(b)]. This gives an alternative electrostatic expression for the optical force between the two metal facets forming a capacitance C across the gap due to the accumulation of opposite charges:

$$F = \frac{1}{2}\left\langle V_g^2 \right\rangle \frac{\partial C}{\partial g} \qquad (2)$$

where V_g is the optical voltage across the feeding gap. Combining Eq. (1) and (2), we obtain the electric field *per photon* inside the gap,

$$\left\langle E_g^2 \right\rangle = \frac{\left\langle V_g^2 \right\rangle}{g^2} = \frac{1}{g^2}\frac{2\hbar\Delta\omega/\Delta g}{\partial C/\partial g} \qquad (3)$$
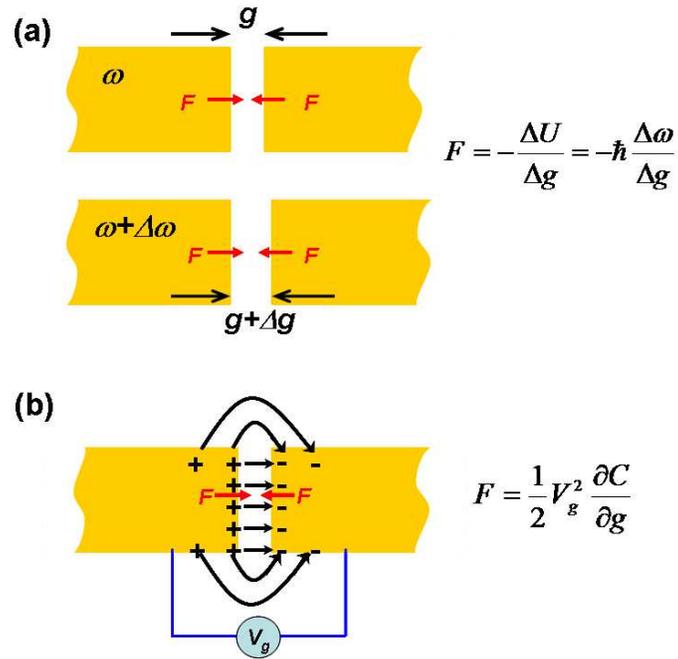

Fig. 1. (a) Schematic of an optical dipole antenna, whose resonance frequency depends on the gap width. The optical force is given as a differentiation of the energy (resonance frequency) with respect to the gap width. (b) In the electro-static picture, the force is a Coulomb force resulting from the opposite charge accumulation on the two electrodes

The mode volume of the plasmonic antenna can be expressed as the ratio between the photon energy and the peak electric energy density (twice the time average) inside the gap [20],

$$V_{eff} = \frac{\hbar\omega}{\varepsilon_0 \left\langle E_g^2 \right\rangle} = \frac{g^2}{2\varepsilon_0}\frac{\partial C}{\partial g}\frac{\omega}{\Delta\omega/\Delta g} \qquad (4)$$

Equation (4) directly relates the mode volume to the relative change of the resonance frequency with respect to the change in gap width g of the antenna. Consequently, this differentiation method, based on far-field measurements of the spectral resonance position, can be used to determine nano-meter scale mode volume.

As a model system, we measure the mode volume of optical loop antennas [21] that consist of a metallic ring with a feeding gap as schematically shown in Fig. 2(a). An analytical formula for the capacitance C across the gap between two metallic electrodes has been developed by taking into account the fringe effect [22,23], yielding (see appendix)

$$\frac{\partial C}{\partial g} \approx -\frac{\varepsilon_0 h w}{g^2} - \frac{\varepsilon_0}{\pi g}[2h + (n_s^2 + 1)w] \tag{5}$$

in the thick electrodes limit (i.e. the thickness of the electrodes along the gap direction is much larger than the gap width g), where n_s is the refractive index of the quartz substrate.
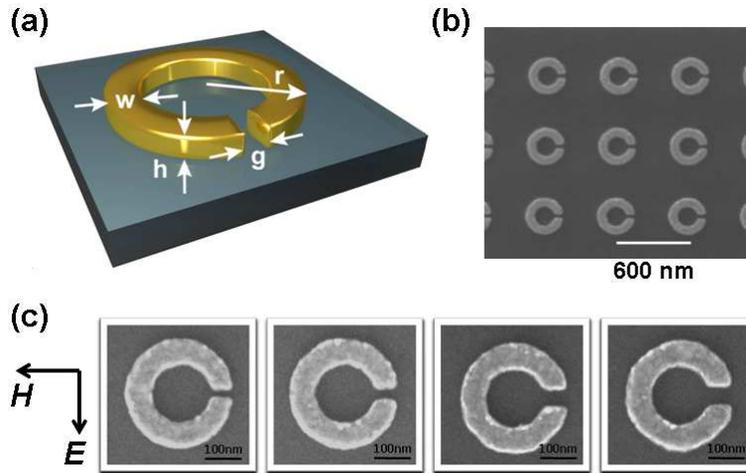

Fig. 2. (a) The schematic of a loop optical antenna. The dimensions are indicated in the figure: The width of the ring W = 68 nm, height of ring h = 40 nm, outer radius r = 155 nm, and the average gap g ranges from 24.1 nm to 54.8 nm for different samples. (b) SEM image of a loop antenna array with a period of 600 nm. (c) SEM images of four different samples with average gap widths of 24.1 nm, 32.1 nm, 45 nm and 54.8 nm, respectively.

The strength of this method is experimentally demonstrated using four different arrays of loop antennas (each array consists of 40x40 elements) on a quartz substrate [Fig. 2(b)], with gap sizes ranging from 24 to 55 nm at a step around 10 nm [Fig. 2(c)]. All the arrays have a period of 600 nm, which is much larger than the size of the loop, such that the near field coupling among the neighboring antennas is negligible. The measured far-field transmission spectra for these arrays are shown in Fig. 3(a). The fundamental resonance can be clearly observed for each sample around 3 µm wavelength. Decreasing the gap width from 55 nm to 24 nm shifts the resonance wavelength from 2.7 µm to 3 µm, and the resonance becomes weaker resulting in shallower transmission dips. According to Eq. (1), the decrease of the resonance frequency (energy) with smaller gaps infers a negative force, or attraction force between the two metal facets, indicating in the electrostatic picture an opposite charge accumulations across the gap. The red-shift of the resonance can also be explained by a simplified LC circuit model, where an increase of capacitance leads to a lower resonance frequency.

To support this observation, we perform numerical simulations of the transmissions using a finite integration technique (FIT) (CST Microwave Studio[TM]), as shown in Fig. 3(b). We found the overall trends in both the peak location and resonance strength are in good agreement with the experimental results, though the simulated transmission spectra show a slight red shift with respect to the measured ones. The electric field plot shown in the inset confirms the strong confinement of the field inside the gap region. In comparison with the simulation, the measured transmission shows slightly broadened resonance features, which could have stemmed from two reasons: the non-uniformity of the loop antennas within one

sample, i.e. inhomogeneous broadening and possible deviation of metal properties from that used in the simulation.

Table 1. Measured gap widths and resonance frequencies

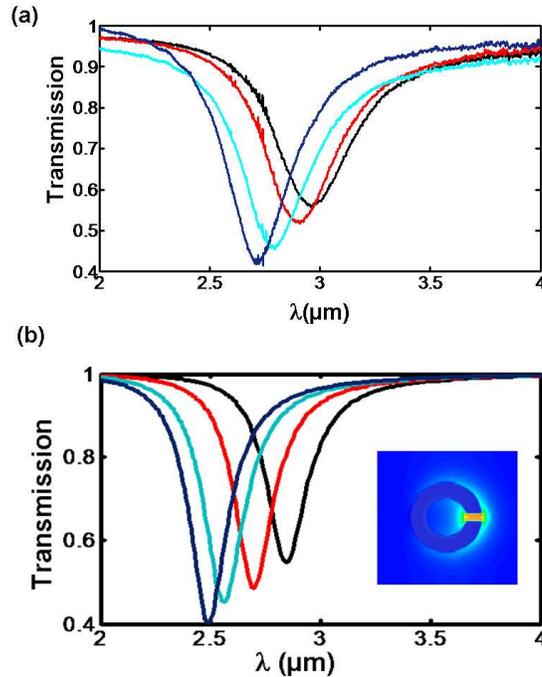| Mean Gap width (nm)	24.11 ± 0.58	32.12 ± 0.84	45.03 ± 0.8	54.78 ± 0.73
Resonance frequency (THz)	101.01	103.45	107.53	110.29

Fig. 3. (a, b) The measured and numerically calculated transmission spectra of samples with average gap width ranging from 24.1 nm to 54.8 nm. In both figures, black, red, cyan and blue curves correspond to samples with increasing gap sizes. The inset in (b) shows the electric field distribution at the resonance frequency (f = 120 THz or λ = 1500 nm) for the loop antenna with gap width of 24.1 nm.

The retrieval of mode volumes using Eq. (4) requires an accurate determination of the *average* gap widths in each sample. Therefore, we have measured the gap width for at least 40 loop antennas on each sample using a scanning electron microscope (SEM), and calculated their average value as well as the uncertainty given as the 95% confidence interval of the sample mean. The average gap widths and the corresponding resonance frequencies for all samples are summarized in Table 1, from which the mode volumes are obtained (Fig. 4, black squares).

The measured mode volumes for all antenna arrays are more than 3 orders of magnitude smaller than λ^3 and increase monotonously with the gap width. Combining with the quality factor ($Q \sim 7$) inferred from the resonance line-width in Fig. 2, the measured mode volumes indicate extremely large Purcell factors ($F_p = \dfrac{3}{4\pi^2}\dfrac{Q}{V_{eff}}\lambda^3$) in the range of 10^3 to 10^4 for emitters placed inside the feeding gap of the antennas. This large enhancement of the Purcell factor is on par with micro-ring and photonic crystal based cavities, albeit with a much lower quality factor. Indeed, nanoplasmonic resonators with large Purcell factors and moderate quality factors are highly desired for achieving light emitting devices with very fast modulation speed.

To complement the experimental measurements, the spectral response of loop antennas with gap ranging from 10 nm to 70 nm at a step of 5 nm was computed using the FIT

simulation whereas the mode volume is calculated from the resonance frequency using the optical force method (Fig. 4, solid blue line). As shown in Fig. 4, this numerically obtained mode volume is in reasonable agreement with the experimental result.

The accuracy of the optical force method was checked by a frequency domain simulation (FEMLAB) that computes the three dimensional electric and magnetic field distribution of the optical mode in the loop antenna. The mode volume was then obtained rigorously as $V_{eff} = \dfrac{U}{\varepsilon_0 \langle \overline{E}^2 \rangle}$, where $\overline{E}$ is the electric field averaged across the gap. U is the total energy stored in the resonator which is given by the summation of both electric and magnetic energy

$$U = \frac{1}{2} \int \left[\frac{d(\omega\varepsilon)}{d\omega} \langle E^2 \rangle + \mu_0 \langle H^2 \rangle \right] d^3 r = \frac{1}{2} \int \left[\frac{d(\omega\varepsilon)}{d\omega} + \varepsilon \right] \langle E^2 \rangle d^3 r$$, with the integration running

over the whole space including air, metal and glass regions. In the above expression, the refractive index of quartz is $n_{sub} = 1.45$, and the permittivity of gold is described by a Drude model with $\varepsilon_\infty = 5.7$, $\omega_p = 1.366 \times 10^{16} \, rad \cdot s^{-1}$ and $\gamma = 9.1 \times 10^{13}$ Hz. The rigorous method yields similar results as the numerical mode volume calculated by the optical force method at small gaps, where the expression of the capacitance across the gap (Eq. (5) is accurate. At larger gaps, the optical force method tends to deviate from the rigorous calculation. Nevertheless, even for the gap width around 50 nm, which is larger than the height of the gap (40 nm), the relative mode volume difference between these two numerical methods is less than 30%, which corresponds to around 10% difference along each dimension. This verifies that the optical force method gives very good quantitative match to the real mode volume, and thus serves as a reliable way for the characterization of the mode volume of plasmonic antennas.
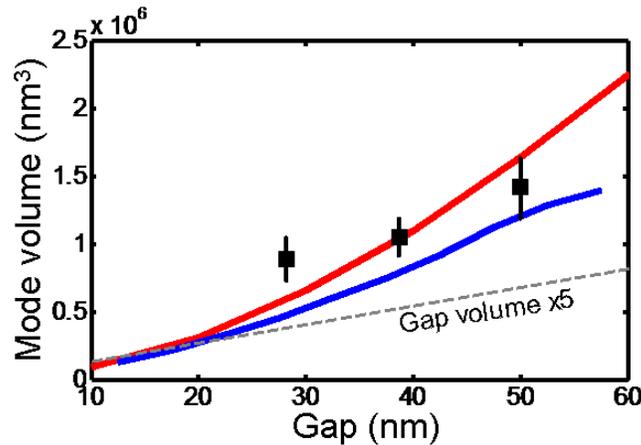

Fig. 4. Measured and simulated mode volumes of loop antennas. The black square and blue solid line represent the mode volume extracted using the optical force method from the resonance frequencies obtained from measurement and Microwave Studio simulation, respectively. The red solid line corresponds to the mode volume calculated rigorously from the near field electric and magnetic field distribution of the eigen-mode. For comparison, the geometrical gap volume, calculated as $V_{gap} = gwh$, is shown as the gray dashed line.

In a conventional *LC* circuit operating in the RF region, the total energy stored in the system is equally split between the electric energy and magnetic energy, with all the electric energy concentrated in the capacitor. As a result, the mode volume is expected to be the same as the volume of the plate capacitor, i.e. the gap volume. However, we found that both the calculated and measured mode volumes were 5-10 times larger than the volume of the gap itself. This is partly due to the fringe effect of the gap capacitor [23]. In addition, the quasi-static model of the loop antenna breaks down since the diameter of the ring is not much less

than the wavelength. Consequently, the loop cannot be considered as a single inductor, but rather a distributed LC element. As a result, there is considerable spreading of the electric field around the metal loop, further increasing the mode volume of the loop antenna.

In conclusion, we have developed an optical force method to measure the mode volume of plasmonic nano antennas with deep sub-wavelength optical confinement in all three dimensions. We implement this method to experimentally determine the mode volume of plasmonic loop antennas operating at the mid-infrared spectral region. The mode volumes were shown to be at least three orders of magnitude less than λ^3, leading to an estimation of extremely large Purcell factors. The optical antennas, with suitable gain medium placed inside their feeding gap, will lead to enormous enhancement of the spontaneous emissions.

Appendix

The derivation of Eq. (5) is based on Ref. 22, in which, the capacitance formed by an electrode above a ground plane was derived [Fig. 5(a)]. In the thick electrode limit ($p \gg g'$), the contribution from the back side of the electrode can be ignored, and the capacitance is given as,

$$C_1(g') \approx \varepsilon_0 \frac{A}{g'} + \frac{\varepsilon_0}{\pi}(\ln a + 0.613)S \qquad (6)$$

$$a = -1 + 2k^2 + 2k\sqrt{k^2 - 1} \approx 4k^2$$

$$k = (p + g')/g' \approx p/g'$$

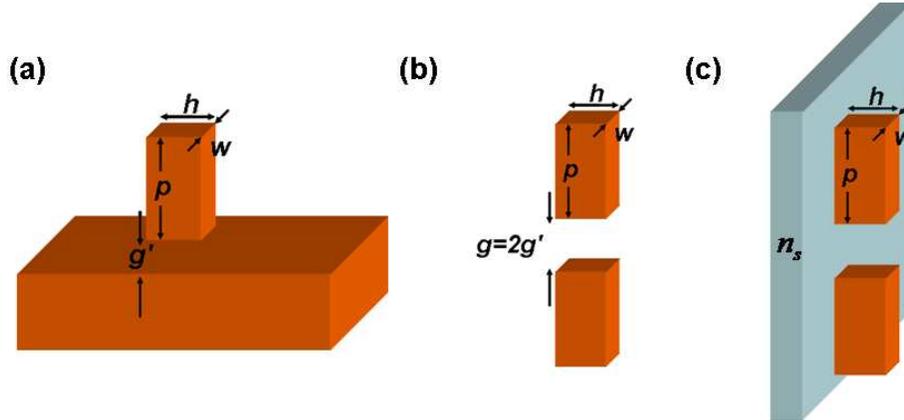where $A = hw$ and $S = 2(h + w)$ are the area and perimeter of the electrode, respectively.

Fig. 5. (a) the schematic of an electrode above a ground plane. (b) the capacitor formed between two identical electrode with twice the gap size as in (a). (c) The capacitor is in touch with a dielectric waveguide (substrate).

The charge distribution and electric field pattern would not be affected if the ground plane is replaced by an image electrode with a separation $g = 2g'$ [Fig. 5(b)]. The capacitance between the two electrodes is therefore half of that between the electrode and ground plane, i.e.

$$C_2(g) = C_1(g')/2 \approx \varepsilon_0 \frac{A}{g} + \frac{\varepsilon_0}{2\pi}(\ln a + 0.613)(2h + 2w) \qquad (7)$$

The capacitance between the two electrodes needs to be modified in the case that one side of the electrodes is in touch with a dielectric slab (substrate), as in Fig. 5(c). The edge

capacitance from that side is therefore scaled by the permittivity (n_s^2) of the substrate, yielding

$$C(g) \approx \varepsilon_0 \frac{A}{g} + \frac{\varepsilon_0}{2\pi}(\ln a + 0.613)[2h + (1+n_s^2)w] \tag{8}$$

Combining Eq. (8) and the definition of parameter a in Eq. (6), it is straight-forward to derive Eq. (5) by taking the derivative of both sides of Eq. (8) with respect to the gap size g.

Acknowledgments